Turk J Elec Eng & Comp Sci, Vol.17, No.3, 2009, © TÜBİTAK
doi:10.3906/elk-0908-186

Construction and applications of the Dirichlet-to-Neumann operator in transmission line modeling

Thomas DEMEESTER*, Daniël DE ZUTTER
Department of Information Technology, Ghent University, Sint-Pietersnieuwstraat 41, B-9000 Ghent, BELGIUM
e-mail: thomas.demeester@intec.ugent.be, daniel.dezutter@intec.ugent.be

Abstract

The Dirichlet-to-Neumann (DtN) operator is a useful tool in the characterization of interconnect structures. In combination with the Method of Moments, it can be used for the calculation of the per-unit length transmission line parameters of multi-conductor interconnections, or to directly determine the internal impedance of conductors. This paper presents a new and fast calculation method for the DtN boundary operator in the important case of rectangular structures, based on the superposition of parallel-plate waveguide modes. Especially for its non-differential form, some numerical issues need to be addressed. It is further explained how the DtN operator can be determined for composite geometries. The theory is illustrated with some numerical examples.

1. Introduction

For accurate signal integrity simulations of on-chip interconnect structures, a broadband transmission line model is required. In the near future, systems with speeds of 40 Gbit/s and higher will be developed, for which undesired effects as cross-talk, losses, and wave propagation on interconnects will play an important role. On printed circuit boards (PCB) at these frequencies, the skin effect is strongly developed, leading to highly increased losses, and taking into account wave propagation effects is eminently important for signal integrity predictions. Sources and loads should therefore be carefully matched, up to the highest frequencies. In order to predict all these effects, an advanced transmission line model is required, rigorously taking into account the material properties and geometry of the considered structures.

In [1], such a 2-D multi-conductor transmission line model is developed for the determination of the quasi-TM resistance, inductance, capacitance and conductance matrices of the system. All homogeneous materials (including dielectrics, conductors and semi-conductors) are replaced by an equivalent contrast current source

*T. Demeester is a research fellow of the Research Foundation - Flanders

in free space. These sources can be transformed into surface sources, resulting in a boundary integral equation formulation of the problem. Essential herein, is the use of the Dirichlet-to-Neumann boundary operator (as introduced below), which allows to deal with a large variation in geometry parameters, see Section 3-B. The boundary formulation is advantageous with respect to other methods that are based on a volume discretization, such as the single-conductor model presented in [2], based on a combination of the Method of Moments and the Method of Lines.

In [1], the transmission line characterization is split up into two parts. For the resistance-inductance (RL) problem, the contrast currents are transformed into differential surface currents j_s on the boundary of conductors and semi-conductors, defined for $e^{j\omega t}$-dependence of the fields, as [3]

$$j_s(r) = \frac{1}{j\omega\mu_0}\left(\frac{\partial e_z(r)}{\partial n} - \frac{\partial e_{z0}(r)}{\partial n}\right), r \in c, \tag{1}$$

with $\partial/\partial n$ the outward normal derivative with respect to the boundary c of the considered material S. e_z satisfies the diffusion equation $\nabla_t^2 e_z = j\omega\mu_0\sigma e_z$ (with the index t denoting the transverse xy-plane), whereas e_{z0} is defined with the same boundary value on c, but in free space, and satisfies Laplace's equation $\nabla_t^2 e_{z0} = 0$ inside S. For the capacitance-conductance (CG) problem, the contrast sources lead to the surface charge on the conductors, and an equivalent surface charge

$$\rho_s(r) = \left(\varepsilon - \varepsilon_0 + \frac{\sigma}{j\omega}\right) \frac{\partial\phi(r)}{\partial n}, r \in c, \tag{2}$$

on the boundaries of dielectrics and semi-conductors. ϕ is the scalar electric potential, satisfying Laplace's equation or the diffusion equation in, respectively, dielectrics and semi-conductors. Consequently, the transformed problem only uses frequency-dependent surface currents and charges in free space, and can be directly solved with the Method of Moments (MoM). For further details, the reader is referred to [1].

The DtN operators D and D_0 are essential in both the RL and the CG problem and are defined, for $r \in c$, by

$$\frac{\partial\psi(r)}{\partial n} = \oint_c D(r,r')\ \psi(r')\ dc', r \in c \tag{3}$$

$$\frac{\partial\psi_0(r)}{\partial n} = \oint_c D_0(r,r')\ \psi_0(r')\ dc', r \in c, \tag{4}$$

with

$$\nabla_t^2\psi(r) = j\omega\mu_0\sigma\ \psi(r) \text{ and } \nabla_t^2\psi_0(r) = 0, r \in S. \tag{5}$$

Hence (1) and (2) can be written concisely as

$$j\omega\mu_0\ j_{s,c} = \oint_c (D - D_0)\ e_z\, dc \tag{6}$$

$$\rho_s(r) = \left(\varepsilon - \varepsilon_0 + \frac{\sigma}{j\omega}\right) \oint_c D\ \phi\, dc, \tag{7}$$

with lower index c to denote evaluation on the considered boundary.

Section 2 deals with the discretization of $(D - D_0)$, in the sequel called the *differential* DtN operator, and D, the *non-differential* DtN operator, on the boundary of a rectangular area, with an extension to arbitrary shapes which are composed of rectangular blocks. In section 3 some applications are discussed, including internal impedance calculations and transmission line modeling. Finally, some conclusions are formulated in Section 4.

2. Construction of the Dirichlet-to-Neumann operator

In [3], a method to calculate the MoM matrix discretization of $(D - D_0)$ for the rectangular area S is proposed, based on the following strategy. A general boundary function ψ expanded in piecewise constant basis functions is projected on a basis of the Dirichlet eigenfunctions of S, resulting for a rectangle in a double summation of sine functions. Next, the normal derivative of each Dirichlet function is calculated, and the double summation is again weighted with the original basis functions, resulting in an expression for $\partial\psi/\partial n$. For the contribution of ψ on one side, to $\partial\psi/\partial n$ on the same or the opposite side, the remaining double summation can be transformed into a single sum. For the interaction between adjacent sides however, a double infinite summation remains, each to be judiciously truncated. The proposed method in this paper directly leads to a single summation for all interactions, and, hence, a much faster calculation. Another reason to introduce the new calculation method presented in this paper, is the need for the non-differential DtN operator in the CG problem, which was not required for the RL problem treated in [3]. The function $(e_z - e_{z0})$, the Dirichlet expansion of which is needed to discretize (6), is zero on c, and the Dirichlet functions of S are indeed only complete on S including its boundary, for the expansion of a function with a zero boundary value. The Dirichlet expansion of ψ with a non-zero boundary value, needed for (7), would lead to an important Gibbs phenomenon on the *total* boundary c, leading to highly inaccurate results. This problem is circumvented with the new method, as will be shown in the next paragraphs.

2.1. Rectangular cross-section

Consider region $S \leftrightarrow x \in [0\,,\,x_0]\ ,\ y \in [0\,,\,y_0]$, with boundary c and sides $c_1(y = 0)$, $c_2(x = x_0)$, $c_3(y = y_0)$, $c_4(x = 0)$. The aim is to determine the discretized (matrix) form of operator D, for which

$$\frac{\partial\psi\,(r)}{\partial n} = \oint_c D\,(r, r')\ \psi\,(r')\ dc', r\ \in\ c \tag{8}$$

$$\nabla_t^2\,\psi\,(r) = -k^2\,\psi\,(r)\,, r\ \in\ S, \tag{9}$$

with $r = x\,u_x + y\,u_y$ the position vector in the chosen $(x; y)$ system. First, an expansion of ψ is constructed from the knowledge of its boundary value ψ_c and based on (9). The contribution of each side is treated separately, by splitting up ψ as

$$\psi\,(x, y) = \sum_{i=1}^{4} \psi^{(i)}\,(x, y), \tag{10}$$

in which $\psi^{(i)}$ takes the actual boundary value of ψ on side c_i, and is zero on the other sides. Expanding ψ on c_1 (written as ψ_{c_1}) into sines immediately leads to

$$\psi^{(1)}(x,y) = \sum_{n=1}^{N_1} A_n^{(1)} \sin\left(\frac{n\pi x}{x_0}\right) \; f_n^-(y/y_0), \tag{11}$$

with $f_n^-(s)$, for $s \in [0,\,1]$, defined as

$$f_n^-(s) = \frac{e^{j\beta_n y_0 s} - e^{j\beta_n y_0 (2-s)}}{1 - e^{j\beta_n 2y_0}} \text{ and } f_n^+(s) = \frac{e^{j\beta_n y_0 s} + e^{j\beta_n y_0 (2-s)}}{1 - e^{j\beta_n 2y_0}} \tag{12}$$

The function f_n^+ is introduced as well, as it will be needed in the sequel. The upper limit N_1 in (11) is taken high enough, such that the truncated sine expansion on c_1 is a good approximation of the actual boundary value of $\psi^{(1)}$. The β_n in (12) are found from

$$\beta_n^2 = k^2 - \left(\frac{n\pi}{x_0}\right)^2, \tag{13}$$

and the square root is chosen such that $\Re(j\beta_n) < 0$. As required, (11) satisfies (9), reduces to

$$\psi_{c_1}^{(1)} = \sum_{n=1}^{N_1} A_n^{(1)} \sin\left(\frac{n\pi\, x}{x_0}\right) \tag{14}$$

on c_1, and is zero on the other sides. Expansion (11) can be seen as an expansion in the modes of a parallel-plate waveguide with c_2 and c_4 as its plates, more specifically these modes that are zero on c_3. The functions $\psi^{(i)}$ (i = *2,3,4*) are defined analogously to (11), but with the sine expansions on the corresponding sides c_i, respectively, and with an analogous interpretation in terms of an expansion in waveguide modes.

Along each side, we will use the normalized coordinate $s \in [0,\,1]$ (in counter-clockwise direction), such that the sides are determined by

$$c_1 \leftrightarrow \{\, x = s\, x_0 \;,\; y = 0 \,\} \tag{15}$$

$$c_2 \leftrightarrow \{\, x = x_0 \;,\; y = s\, y_0 \,\} \tag{16}$$

$$c_3 \leftrightarrow \{\, x = (1-s)\; x_0 \;,\; y = y_0 \,\} \tag{17}$$

$$c_4 \leftrightarrow \{\, x = 0 \;,\; y = (1-s)\; y_0 \,\}. \tag{18}$$

In order to discretize ψ on c_1, this side is divided into M_1 segments, using the discretization points x_m, (m = *1,...,* $M_1 + 1$), not necessarily chosen uniformly along c_1, and with x_1 and x_{M_1+1} the corner points. The normalized coordinates of these discretization points are $s_m = x_m/x_0$, such that $s_1 = 0$ and $s_{M_1+1} = 1$. An analogous discretization is performed for the other sides, with the segments numbered in counter-clockwise direction. On side c_i (i = *1,2,3,4*), ψ_{c_i} can hence be approximated by

$$\psi_{c_i}(s) \cong \sum_{m=1}^{M_i} \Psi_{c_i,m}\, t_{c_i,m}(s). \tag{19}$$

The basis functions $t_{c_i,m}(s)$, with $m = 1,\ldots,\ M_i$, can be a constant pulse on the interval $[s_m,\ s_{m+1}]$ (corresponding, e.g. on c_1, to $x \in [x_m,\ x_{m+1}]$), a piecewise linear 'hat' function on $[s_{m-1},\ s_{m+1}]$, or any other basis function. The coefficients $\Psi_{c_i,m}$ are taken together into one column vector Ψ_c as

$$\Psi_c = \begin{bmatrix} \Psi_{c_1} \\ \Psi_{c_2} \\ \Psi_{c_3} \\ \Psi_{c_4} \end{bmatrix} \text{ with } \left[\Psi_{c_i}\right]_m = \Psi_{c_i,m}. \tag{20}$$

In a first step, the expansion coefficients $A_n^{(1)}$ from (11) (and grouped in the vector $A^{(1)}$) are determined from the coefficients $\Psi_{c_1,m}$. By inserting (15) in (11), we find with (19)

$$\psi_{c_1}^{(1)} \cong \sum_{m=1}^{M_1} \Psi_{c_1,m}\, t_{c_1,m}\,(s) \cong \sum_{n=1}^{N_1} A_n^{(1)}\ \sin\left(n\pi s\right), \tag{21}$$

and, by weighting with the set $\{2\ \sin n\pi\, s\}$,

$$Q_1 \cdot \Psi_{c_1} = A^{(1)}. \tag{22}$$

The $N_1 \times M_1$ matrix Q_1 is given by

$$\left[Q_1\right]_{n,m} = 2 \int_0^1 t_{c_1,m}\,(s)\ \sin\left(n\pi s\right)\ ds. \tag{23}$$

The knowledge of the coefficients $A_n^{(1)}$ determines the normal derivative of $\psi^{(1)}$ on each side of S. We find from (11), invoking (12) and (15–18),

$$\frac{\partial \psi_{c_1}^{(1)}\,(s)}{\partial n} = \sum_{n=1}^{N_1} -j\beta_n\, f_n^+\,(0)\ \ \sin\left(n\pi s\right)\ A_n^{(1)} \tag{24}$$

$$\frac{\partial \psi_{c_2}^{(1)}\,(s)}{\partial n} = \sum_{n=1}^{N_1} \frac{n\pi}{x_0}\ (-1)^n\, f_n^-\,(s)\ A_n^{(1)} \tag{25}$$

$$\frac{\partial \psi_{c_3}^{(1)}\,(s)}{\partial n} = \sum_{n=1}^{N_1} j\beta_n\, f_n^+\,(1)\ \ \sin\left(n\pi\,(1-s)\right)\ A_n^{(1)} \tag{26}$$

$$\frac{\partial \psi_{c_4}^{(1)}\,(s)}{\partial n} = \sum_{n=1}^{N_1} -\frac{n\pi}{x_0}\, f_n^-\,(1-s)\ A_n^{(1)}. \tag{27}$$

The normal derivative $\partial\psi^{(1)}/\partial n$ is discretized on side c_i as

$$\frac{\partial \psi_{c_i}^{(1)}\,(s)}{\partial n} \cong \sum_{m=1}^{M_i} \Gamma_{c_i,m}^{(1)}\, t_{c_i,m}\,(s)\,, \tag{28}$$

and weighting (24)–(27) with the basis functions $t_{c_i,m}(s)$ on the corresponding sides, leads with (28) to

$$B_i \cdot \Gamma_{c_i}^{(1)} = T_{i1} \cdot A^{(1)}, i = 1, \ldots, 4, \tag{29}$$

with the $M_i \times M_i$ weighting matrices B_i given by

$$[B_i]_{m,\tilde{m}} = \int_0^1 t_{c_i,m}(s)\ t_{c_i,\tilde{m}}(s)\ ds, \tag{30}$$

and the $M_i \times N_1$ submatrices T_{i1} given by

$$[T_{11}]_{\tilde{m},n} = -j\beta_n f_n^+(0) \int_0^1 \sin(n\pi s)\ t_{c_1,\tilde{m}}(s)\ ds \tag{31}$$

$$[T_{21}]_{\tilde{m},n} = \frac{n\pi}{x_0}(-1)^n \int_0^1 f_n^-(s)\ t_{c_2,\tilde{m}}(s)\ ds \tag{32}$$

$$[T_{31}]_{\tilde{m},n} = j\beta_n f_n^+(1) \int_0^1 \sin(n\pi(1-s))\ t_{c_3,\tilde{m}}(s)\ ds \tag{33}$$

$$[T_{41}]_{\tilde{m},n} = -\frac{n\pi}{x_0} \int_0^1 f_n^-(1-s)\ t_{c_4,\tilde{m}}(s)\ ds. \tag{34}$$

Finally, with (22) and (29),

$$\Gamma_c^{(1)} = D^{(1)} \cdot \Psi_{c_1} \tag{35}$$

for

$$\Gamma_c^{(1)} = \begin{bmatrix} \Gamma_{c_1}^{(1)} \\ \Gamma_{c21}^{(1)} \\ \Gamma_{c3}^{(1)} \\ \Gamma_{c_4}^{(1)} \end{bmatrix} \text{ and } D^{(1)} = \begin{bmatrix} B_1^{-1} T_{11} \\ B_2^{-1} T_{21} \\ B_3^{-1} T_{31} \\ B_4^{-1} T_{41} \end{bmatrix} \cdot Q_1 \tag{36}$$

The matrix $D^{(1)}$ maps the boundary value of $\psi^{(1)}$, i.e., the actual value of ψ on c_1 and zero on the other sides, onto its normal derivative $\partial\psi_c^{(1)}/\partial n$. A similar procedure yields the matrices $D^{(2)}$, $D^{(3)}$, and $D^{(4)}$ to account for the boundary value of ψ on sides c_2, c_3, and c_4. The total DtN matrix D can hence be constructed, with (20), as

$$D = \left[D^{(1)}\ D^{(2)}\ D^{(3)}\ D^{(4)} \right]. \tag{37}$$

The calculation as described above for the non-differential matrix D (or D_0), raises an accuracy problem in the corners of the rectangle. The sine expansion on each side is actually the Fourier series of the "odd

extension" of ψ on that side, and hence discontinuous in case the corner values are non-zero. This causes a Gibbs phenomenon that is reinforced in the calculation of $\partial\psi/\partial n$, and leads to an inaccurate D. However, a well-chosen mathematical manipulation allows to circumvent this problem. Let us first discuss the calculation of the non-differential matrix D_0. A part $\tilde{\psi}_0 = p_1 xy + p_2 x + p_3 y + p_4$ is beforehand subtracted from the total ψ_0, as it obviously satisfies Laplace's equation, and with the coefficients p_i chosen such, that in the four corners $\tilde{\psi}_0 = \psi_0$ (assuming ψ continuous along the boundary, which is indeed the case for both the electric scalar potential and for the longitudinal electric field). The normal derivative of $\tilde{\psi}_0$ is known analytically, and the technique described above is then used for the calculation of $\partial\left(\psi_0 - \tilde{\psi}_0\right)/\partial n$, immune to Gibbs phenomena as the corner values are identically zero.

The differential DtN matrix $(D - D_0)$ is also calculated with the procedure explained in this section, but with the submatrices $(T_{ij} - T_{ij,0})$ instead of only T_{ij}. A careful calculation of these submatrices allows to take into account the fact that $\psi_c - \psi_{0,c} = 0$, such that no Gibbs phenomenon will be present, and $(D - D_0)$ is accurate.

Finally, D can be calculated by adding D_0 to $(D - D_0)$. Alternatively, D can be calculated *directly* as well. There always exists an analytically known function $\tilde{\psi}$ which has the same corner values as ψ itself, and satisfies the diffusion equation (9) inside S, for any value of k^2. Such a function $\tilde{\psi}$ can be formed as a linear combination of four functions $\tilde{\psi}^{p_i}$ $(i = 1,\ldots,4)$, which are 1 in corner p_i but zero in all the other corners, and satisfy (9) inside S. Such a function is, e.g., for corner $p_1(0,0)$

$$\tilde{\psi}^{p_1}(x,y) = \cos\left(\frac{\pi x}{2x_0}\right)\left(\frac{e^{j\beta y} - e^{j\beta(2y_0 - y)}}{1 - e^{j\beta 2y_0}}\right), \tag{38}$$

with $\beta^2 = k^2 - (\pi/2x_0)^2$, and analogous for the other corners. The numerical procedure to determine the DtN operator can then be correctly applied to $\left(\psi - \tilde{\psi}\right)$, and the normal derivative of $\tilde{\psi}$ can be calculated separately, again leading to the correct DtN operator.

An example is given to illustrate the explained ideas. Figure 1 shows the normal derivative of a harmonic function ψ_0 of the form

$$\psi_0(x,y) = \alpha_1\left(\cos cx + \alpha_2 \sin cx\right)\left(e^{cy} + \alpha_3 e^{-cy}\right) + \alpha_4 \tag{39}$$

on the boundary of rectangle S, shown in the inset of Figure 1. The coefficients α_1 to α_4 can be determined from the arbitrarily chosen value $c = 3\pi/2$, together with the indicated corner values of ψ_0 in Figure 1. A fine discretization was used (horizontally 100 intervals and 1000 sines, vertically 30 intervals and 300 sines). The analytical normal derivative, $\partial\psi_0/\partial n$, is compared to the result with the compensation for non-zero boundary values of ψ_0, indicated in Figure 1 as "ψ_0 indirect", and the results are indistinguishable. Conversely, the method without compensation, denoted "ψ_0 direct", exhibits, as expected, an important Gibbs phenomenon in the three corners where $\psi_0 \neq 0$.

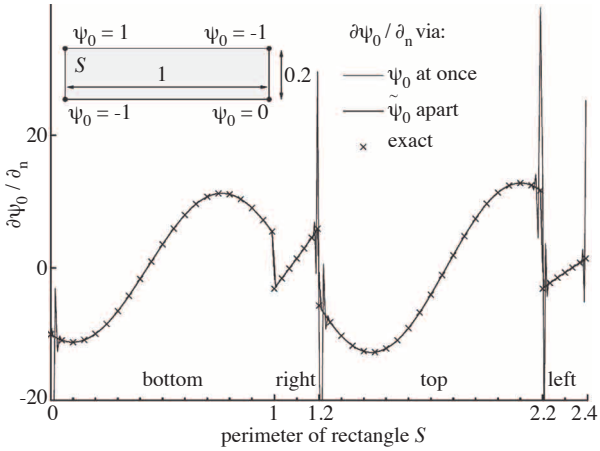

Figure 1. Normal derivative of a harmonic function ψ_0. For "ψ_0 direct", $\partial\psi_0/\partial n$ was calculated as $\oint\limits_c D_0\,\psi_0\,dc$, whereas for "$\psi_0$ indirect", as $\partial\tilde{\psi}_0/\partial n + \oint\limits_c D_0\left(\psi_0 - \tilde{\psi}_0\right)dc$.

2.2. General cross-sections

The following paragraphs describe how the matrix D_{tot}, i.e., the discretized form of the total DtN operator, can be calculated for a general shape that consists of parts for which the matrix D is known. A distinction has to be made between the discretization of $\partial e_z/\partial n$ (for conductors) and $\partial\phi/\partial n$ (for dielectrics), with e_z the longitudinal electric field, and ϕ the scalar electric potential.

In the case of a composite conductor, the matrix D_{tot} can be obtained from the matrices $D^{(i)}$ of the different parts of the conductor (for which the conductivity $\sigma^{(i)}$ is assumed constant) by elimination of the internal boundaries. To that end, two additional conditions have to be imposed, i.e., the continuity of both e_z and $\partial e_z/\partial n$ on the internal boundaries. In the quasi-TM approximation $\partial e_z/\partial n$ is continuous, due to the continuity of the cross-sectional tangential magnetic field

$$h_{\tan} \cong \frac{1}{j\omega\mu_0}\left(\frac{\partial e_z}{\partial n} - \frac{1}{\sigma}\frac{\partial^2 h_z}{\partial z\,\partial\tan}\right) \cong \frac{1}{j\omega\mu_0}\frac{\partial e_z}{\partial n} \tag{40}$$

For the determination of the differential surface admittance matrix $Y_{tot} = \left(D_{tot} - D_{0,tot}\right)/j\omega\mu_0$ of a composite conductor [4], D_{tot} and $D_{0,tot}$ need to be determined separately from the corresponding matrices of the different parts. The reason is that e_z (satisfying the diffusion equation) and e_{z0} (satisfying Laplace's equation) are not the same on the inner boundaries of the total conductor (although they need to be identical on the outer boundary, by definition).

In order to calculate the discretized form of $\partial\phi/\partial n$ for composite dielectrics, the continuity of ϕ needs to be invoked, as well as the continuity of $(\varepsilon + \sigma/j\omega)\ \partial\phi/\partial n$, because for these materials $\boldsymbol{e}_t \approx -\nabla_t\,\phi$ within the quasi-TM approximation [1].

3. Applications of the Dirichlet-to-Neumann operator

3.1. Internal impedance calculations

Consider a conductor above a reference plane, situated infinitely far away (in order to exclude proximity effects). The current I through the conductor can be written, because e_z inside the conductor satisfies the diffusion equation, as

$$I = \iint_S \sigma\, e_z\, dS = \frac{1}{j\omega\mu_0} \oint_c \frac{\partial e_z}{\partial n}\, dc = -\frac{1}{j\omega\mu_0} \oint_c dc \oint_c D \left(\frac{\partial V}{\partial z} + j\omega\, a_z \right) dc, \tag{41}$$

in which V is the constant boundary value of the electric scalar potential ϕ, and a_z the longitudinal component of the magnetic vector potential. In order to determine the *internal* impedance, the magnetic field *outside* the conductor should be made zero, or, $a_z = const = 0$ because on the reference at infinity $a_z = 0$. It is physically not possible to have a non-zero current without an external magnetic field. The above reasoning is merely a way to conclude that the influence of the external magnetic field is omitted from (41) by setting $a_z = 0$ on c. The remaining part I_{in} of the current is related to the internal impedance Z_{in} by $\partial V/\partial z = -Z_{in}\, I_{in}$, such that Z_{in} can be identified as

$$Z_{in}^{-1} = \frac{1}{j\omega\,\mu_0} \oint_c dc \oint_c D\, dc\,. \tag{42}$$

Hence the DtN operator directly leads to the internal impedance of a conductor. It can be proven that, for the case of a homogeneous rectangular conductor, (42) is identical to the result obtained in [5]. For more details, and a comparison with an alternative calculation method for the internal impedance, the reader is referred to [6].

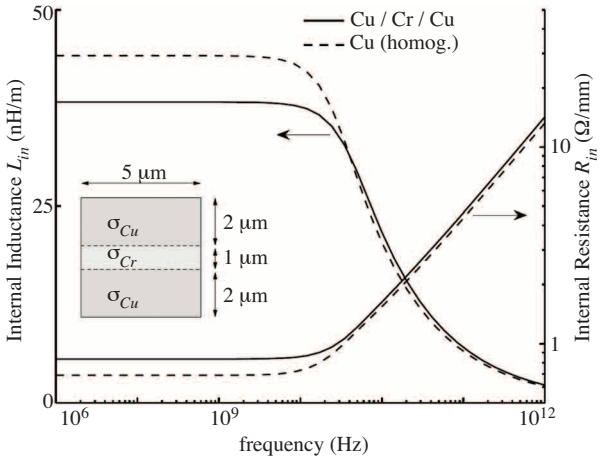

Figure 2. Internal inductance L_{in} and internal resistance R_{in} for a layered conductor (σ_{Cu}= 58 MS/m, σ_{Cr} = 7.75 MS/m), compared to a homogeneous copper conductor.

Consider the layered conductor shown in the inset of Figure 2. The circuit behavior of such a conductor in a micro-strip configuration was described in [4]. It is now possible to investigate the influence of the inhomogeneity, by determining Z_{in}. To that end, the total DtN operator for the composite conductor is

calculated, and then with (42) the internal impedance $Z_{in} = R_{in} + j\omega L_{in}$. The result is shown in Figure 2, where the layered conductor is compared to a homogeneous copper conductor with the same geometry.

4. Transmission line modeling

A complete on-chip transmission line configuration is shown in Figure 3. Two pairs of parallel traces, (c_1, c_2) and (c_3, c_4), are embedded in a dielectric material above a semi-conducting substrate. The DtN operator is used to replace conductors, semi-conductors and dielectrics by surface sources in free space, from which the transmission line parameters are determined.

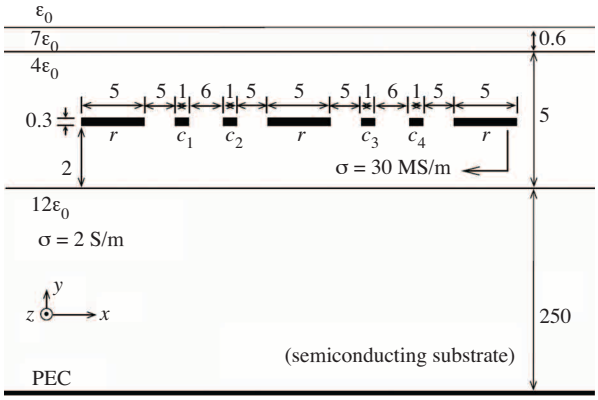

Figure 3. Cross section (not drawn to scale) of a four-line configuration (conductors c_1 to c_4), with three reference conductors (indicated as r). All dimensions are in micrometers.

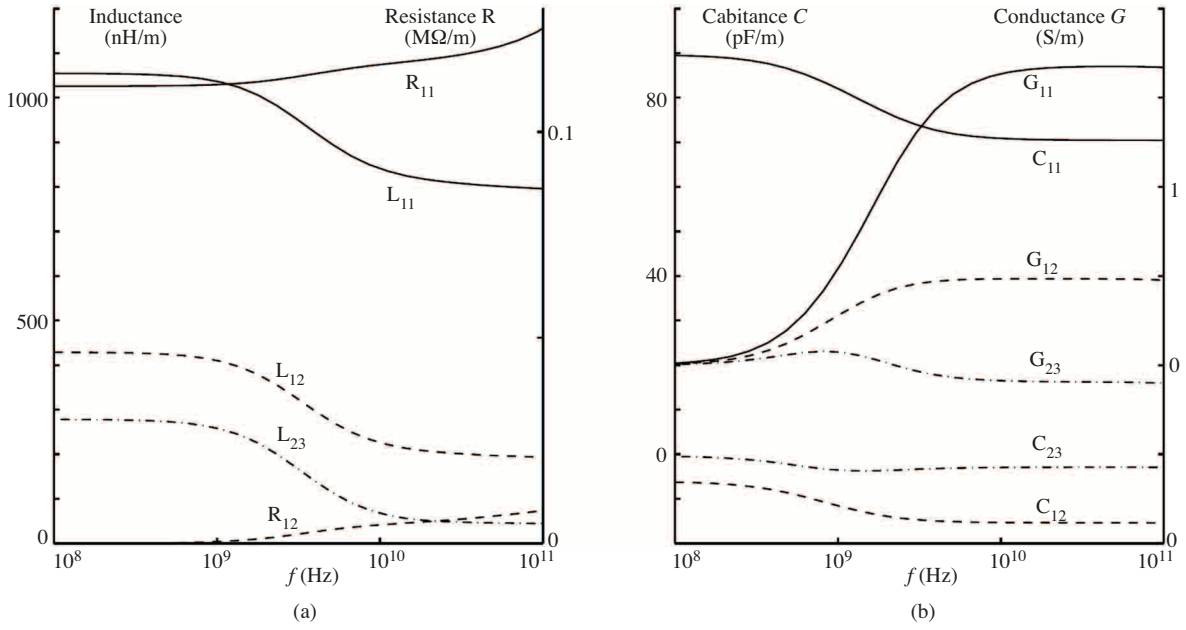

Figure 4. Elements of the transmission line matrices (a) inductance and resistance, and (b) capacitance and conductance, for the structure of Figure 3.

Some elements of the resulting transmission line matrices per unit length (the inductance L, resistance R, capacitance C, and conductance G) are shown in Figure 4. In Figure 4 (a), the inductance elements show that at the highest frequencies the magnetic field is for the greater part forced out of the conductors. This corresponds to the current crowding effect, resulting in an increased resistance R_{11}. The skin effect is not yet fully developed though, as at 100 GHz the skin-depth equals the conductors' height. Figure 4 (b) shows the capacitance and conductance elements. As motivated in [1], a material is considered a good conductor as long as its conductivity $\sigma >> \omega\varepsilon$. If that is the case for the semi-conducting substrate, i.e., if the frequency is low enough, a surface charge exists on top of the substrate. At 100 MHz, this surface charge is still considerable ($\sigma_s \approx 30\,\omega\varepsilon$, with $\sigma_s = 2$ S/m and $\varepsilon = 12\,\varepsilon_0$), but at 3 GHz, $\sigma_s \approx \omega\varepsilon$, and from higher frequencies onwards, the substrate behaves as a dielectric. The presence of this low-frequency surface charge on the substrate increases the self-capacitance C_{11} but at the same time has a decoupling effect on the nearby conductors. This explains why $|C_{12}|$ and $|C_{23}|$ increase when the substrate starts to behave as a dielectric. It is also observed that the self-conductance G_{11} increases once the dielectric behavior of the substrate becomes dominant, because then a transverse electric field is built up inside the substrate, causing the conductance losses.

It is now investigated how the signal line pairs of Figure 3 are coupled, when they are excited with perfectly differential currents. Both signal pairs are separated by a reference conductor r (kept on zero potential). A reference conductor is placed on both sides of the signal lines as well, so as to guarantee as good as possible the symmetry of the configuration, avoiding the excitation of the common modes. First, consider only the conductor pair (c_1, c_2), designed for a high-frequency differential characteristic impedance of 175 Ω (in the absence of other conductors). The separation of 6 μm between c_1 and c_2 is chosen quite large to keep the mutual capacitance low, and as such minimize the attenuation and maximize the propagation speed of the differential mode. The separation cannot become too large, however, to keep the sensitivity with respect to outside noise low.

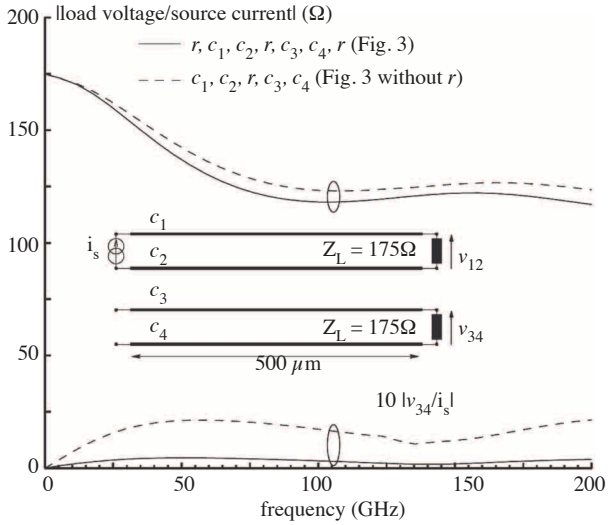

Figure 5. Source-interconnect-load configuration and load voltages, comparing the configuration of Figure 3 with the case in which the reference conductors r are left away.

Suppose two such pairs are used for a 500 μm long on-chip interconnection, but only little space is available, such that c_2 and c_3 can be separated by a distance of 15 μm only, to keep the lines far enough away from other circuits. The inset of Figure 5 shows how the lines are used to connect a source with a differential load impedance of 175 Ω. The results in Figure 5 show the output voltages $|V_{12}|$ and $|V_{34}|$ for a unit current excitation of signal pair (c_1, c_2) and with the current source on the other pair switched off. The configuration of Figure 3 is compared with the case in which the three reference conductors are left out. The coupling of both lines for a differential excitation is, as expected, smaller when the reference conductors r shield the signal lines. Yet the coupling is in both cases very weak (considering the factor 10 in the graphical presentation of $|V_{34}/i_s|$). What's more, the presence of the conductors r increases the capacitance of the signal lines. As a result, see $|V_{12}/i_s|$ in Figure 5, the attenuation gets higher, and the lines become electrically longer, such that wave effects become important from slightly lower frequencies onwards.

5. Conclusion

This paper presents a new and efficient way to calculate the differential Dirichlet-to-Neumann boundary operator for rectangular blocks. Unlike the original calculation method [3], the new method allows to calculate the non-differential DtN operator as well, which is needed on the one hand for capacitance calculations and, on the other hand, to calculate the DtN operator for more complicated shapes. Some numerical examples demonstrate the practical use of the DtN operator for internal impedance calculations and, especially, for accurate transmission line modeling.

References

[1] T. Demeester, D. De Zutter, "Quasi-TM transmission line parameters of coupled lossy lines based on the Dirichlet to Neumann boundary operator," *IEEE Trans. Microwave Theory Tech.*, vol. 56, no. 7, pp. 1649–1660, July 2008.

[2] G. Plaza, R. Marques, F. Medina, "Quasi-TM MoL/MoM approach for computing the transmission-line parameters of lossy lines," *IEEE Trans. Microwave Theory Tech.*, vol. 54, no. 1, pp. 198–209, Jan. 2006.

[3] D. De Zutter, L. Knockaert, "Skin effect modeling based on a differential surface admittance operator," *IEEE Trans. Microwave Theory Tech.*, vol. 53, no. 8, pp. 2526–2538, Aug. 2005.

[4] T. Demeester, D. De Zutter, "Modeling the broadband inductive and resistive behavior of composite conductors," *IEEE Microwave Wireless Compon. Lett.*, vol. 18, no. 4, pp. 230–232, Apr. 2008.

[5] A. Rong, A. Cangellaris, "Note on the definition and calculation of the per-unit-length internal impedance of a uniform conducting wire," *IEEE Trans. Electromagn. Compat.*, vol. 49, no. 3, pp. 677–681, Aug. 2007.

[6] T. Demeester, D. De Zutter, "Internal impedance of composite conductors with arbitrary cross section," *IEEE Trans. Electromagn. Compat.*, vol. 51, no. 1, pp. 101–107, Feb. 2009.